

REPORT DOCUMENTATION PAGE			Form Approved OMB NO. 0704-0188		
<p>The public reporting burden for this collection of information is estimated to average 1 hour per response, including the time for reviewing instructions, searching existing data sources, gathering and maintaining the data needed, and completing and reviewing the collection of information. Send comments regarding this burden estimate or any other aspect of this collection of information, including suggestions for reducing this burden, to Washington Headquarters Services, Directorate for Information Operations and Reports, 1215 Jefferson Davis Highway, Suite 1204, Arlington VA, 22202-4302. Respondents should be aware that notwithstanding any other provision of law, no person shall be subject to any penalty for failing to comply with a collection of information if it does not display a currently valid OMB control number. PLEASE DO NOT RETURN YOUR FORM TO THE ABOVE ADDRESS.</p>					
1. REPORT DATE (DD-MM-YYYY) 15-03-2017		2. REPORT TYPE Final Report		3. DATES COVERED (From - To) 15-Aug-2016 - 14-Feb-2017	
4. TITLE AND SUBTITLE Final Report: Acoustically/Vibrationally Enhanced High Frequency Electromagnetic Detector for Buried Landmines			5a. CONTRACT NUMBER		
			5b. GRANT NUMBER W911NF-16-P-0043		
			5c. PROGRAM ELEMENT NUMBER 665502		
6. AUTHORS David Boutte, Vincent Radzicki, Adam Webb, Brian Thelan, Joseph Burns			5d. PROJECT NUMBER		
			5e. TASK NUMBER		
			5f. WORK UNIT NUMBER		
7. PERFORMING ORGANIZATION NAMES AND ADDRESSES AKELA, Inc. 5551 Ekwill St. Suite A Santa Barbara, CA 93111 -2355			8. PERFORMING ORGANIZATION REPORT NUMBER		
9. SPONSORING/MONITORING AGENCY NAME(S) AND ADDRESS (ES) U.S. Army Research Office P.O. Box 12211 Research Triangle Park, NC 27709-2211			10. SPONSOR/MONITOR'S ACRONYM(S) ARO		
			11. SPONSOR/MONITOR'S REPORT NUMBER(S) 69351-EL-ST1.1		
12. DISTRIBUTION AVAILABILITY STATEMENT Approved for Public Release; Distribution Unlimited					
13. SUPPLEMENTARY NOTES The views, opinions and/or findings contained in this report are those of the author(s) and should not be construed as an official Department of the Army position, policy or decision, unless so designated by other documentation.					
14. ABSTRACT Detection, classification and discrimination of buried landmines and explosive hazards remain open and critically important problems for both soldier protection and mobility and humanitarian remediation. Earlier laboratory investigations have suggested that acoustically or vibrationally inducing motion in buried targets can aid in improving target detectability through a characteristic response related to differential target motion. This gain is realized by adding an additional degree of freedom, modulation due to motion in the GPR return signal, to use as a discriminating feature.					
15. SUBJECT TERMS GPR, vibration, multi-modal, Doppler processing					
16. SECURITY CLASSIFICATION OF:		17. LIMITATION OF ABSTRACT		15. NUMBER OF PAGES	19a. NAME OF RESPONSIBLE PERSON
a. REPORT UU	b. ABSTRACT UU	c. THIS PAGE UU	UU		David Boutte
				19b. TELEPHONE NUMBER 805-683-6414	

Report Title

Final Report: Acoustically/Vibrationally Enhanced High Frequency Electromagnetic Detector for Buried Landmines

ABSTRACT

Detection, classification and discrimination of buried landmines and explosive hazards remain open and critically important problems for both soldier protection and mobility and humanitarian remediation. Earlier laboratory investigations have suggested that acoustically or vibrationally inducing motion in buried targets can aid in improving target detectability through a characteristic response related to differential target motion. This gain is realized by adding an additional degree of freedom, modulation due to motion in the GPR return signal, to use as a discriminating feature.

The AKELA/Michigan Tech Research Institute (MTRI) team has conducted a successful Phase I program resulting in significant phenomenological knowledge, vibratory exploitation algorithm development, full wave modeling and simulation capability, feasibility analysis and performance assessment. Exploiting an induced vibratory response in a buried landmine surrogate was shown to be feasible using a UWB GPR and results in significant SCR improvement over traditional GPR techniques. Similarly, the ability to discriminate both between resonant landmine surrogates as well as between landmine surrogates and discrete clutter based on vibratory frequency response was also demonstrated.

Enter List of papers submitted or published that acknowledge ARO support from the start of the project to the date of this printing. List the papers, including journal references, in the following categories:

(a) Papers published in peer-reviewed journals (N/A for none)

<u>Received</u>	<u>Paper</u>
-----------------	--------------

TOTAL:

Number of Papers published in peer-reviewed journals:

(b) Papers published in non-peer-reviewed journals (N/A for none)

<u>Received</u>	<u>Paper</u>
-----------------	--------------

TOTAL:

Number of Papers published in non peer-reviewed journals:

(c) Presentations

NONE

Number of Presentations: 0.00

Non Peer-Reviewed Conference Proceeding publications (other than abstracts):

Received Paper

TOTAL:

Number of Non Peer-Reviewed Conference Proceeding publications (other than abstracts):

Peer-Reviewed Conference Proceeding publications (other than abstracts):

Received Paper

TOTAL:

Number of Peer-Reviewed Conference Proceeding publications (other than abstracts):

(d) Manuscripts

Received Paper

TOTAL:

Number of Manuscripts:

Books

Received Book

TOTAL:

Received

Book Chapter

TOTAL:

Patents Submitted

NONE

Patents Awarded

NONE

Awards

NONE

Graduate Students

<u>NAME</u>	<u>PERCENT SUPPORTED</u>
FTE Equivalent:	
Total Number:	

Names of Post Doctorates

<u>NAME</u>	<u>PERCENT SUPPORTED</u>
FTE Equivalent:	
Total Number:	

Names of Faculty Supported

<u>NAME</u>	<u>PERCENT SUPPORTED</u>
FTE Equivalent:	
Total Number:	

Names of Under Graduate students supported

<u>NAME</u>	<u>PERCENT SUPPORTED</u>
FTE Equivalent:	
Total Number:	

Student Metrics

This section only applies to graduating undergraduates supported by this agreement in this reporting period

The number of undergraduates funded by this agreement who graduated during this period: 0.00

The number of undergraduates funded by this agreement who graduated during this period with a degree in science, mathematics, engineering, or technology fields:..... 0.00

The number of undergraduates funded by your agreement who graduated during this period and will continue to pursue a graduate or Ph.D. degree in science, mathematics, engineering, or technology fields:..... 0.00

Number of graduating undergraduates who achieved a 3.5 GPA to 4.0 (4.0 max scale):..... 0.00

Number of graduating undergraduates funded by a DoD funded Center of Excellence grant for Education, Research and Engineering:..... 0.00

The number of undergraduates funded by your agreement who graduated during this period and intend to work for the Department of Defense 0.00

The number of undergraduates funded by your agreement who graduated during this period and will receive scholarships or fellowships for further studies in science, mathematics, engineering or technology fields:..... 0.00

Names of Personnel receiving masters degrees

NAME

Total Number:

Names of personnel receiving PHDs

NAME

Total Number:

Names of other research staff

NAME

PERCENT SUPPORTED

FTE Equivalent:

Total Number:

Sub Contractors (DD882)

1 a. Michigan Tech Research Institute

1 b. 1400 Townsend Dr.

Houghton MI 499311295

Sub Contractor Numbers (c):

Patent Clause Number (d-1):

Patent Date (d-2):

Work Description (e): Development of acoustic/seismic simulations to characterize target motion and vibration c

Sub Contract Award Date (f-1): 10/15/16 12:00AM

Sub Contract Est Completion Date(f-2): 2/14/17 12:00AM

1 a. Michigan Tech Research Institute

1 b. 1400 Townsend Dr.

Houghton MI 499311295

Sub Contractor Numbers (c):

Patent Clause Number (d-1):

Patent Date (d-2):

Work Description (e): Development of acoustic/seismic simulations to characterize target motion and vibration c

Sub Contract Award Date (f-1): 10/15/16 12:00AM

Sub Contract Est Completion Date(f-2): 2/14/17 12:00AM

Inventions (DD882)

Scientific Progress

See attached technical report.

Technology Transfer

See final technical report attachment.

REPORT DOCUMENTATION PAGE

Form Approved
OMB No. 0704-0188

The public reporting burden for this collection of information is estimated to average 1 hour per response, including the time for reviewing instructions, searching existing data sources, gathering and maintaining the data needed, and completing and reviewing the collection of information. Send comments regarding this burden estimate or any other aspect of this collection of information, including suggestions for reducing the burden, to Department of Defense, Washington Headquarters Services, Directorate for Information Operations and Reports (0704-0188), 1215 Jefferson Davis Highway, Suite 1204, Arlington, VA 22202-4302. Respondents should be aware that notwithstanding any other provision of law, no person shall be subject to any penalty for failing to comply with a collection of information if it does not display a currently valid OMB control number.
PLEASE DO NOT RETURN YOUR FORM TO THE ABOVE ADDRESS.

1. REPORT DATE (DD-MM-YYYY) 03/15/2017		2. REPORT TYPE Final technical report for W911NF-16-P-0043		3. DATES COVERED (From - To) 08/15/2016-02/14/2017	
4. TITLE AND SUBTITLE Acoustically/Vibrationally Enhanced High Frequency Electromagnetic Detector for Buried Landmines				5a. CONTRACT NUMBER W911NF-16-P-0043	
				5b. GRANT NUMBER	
				5c. PROGRAM ELEMENT NUMBER	
6. AUTHOR(S) David Boutte, Vincent Radzicki, Adam Webb, Brian Thelan, Joseph Burns				5d. PROJECT NUMBER	
				5e. TASK NUMBER	
				5f. WORK UNIT NUMBER	
7. PERFORMING ORGANIZATION NAME(S) AND ADDRESS(ES) AKELA Inc, 5551 Ekwill St. Suite A, Santa Barbara CA. 93111 MTRI, MTU, 3600 Green Ct. Ste. 100, Ann Arbor, MI 48105				8. PERFORMING ORGANIZATION REPORT NUMBER W911NF-16- P-0043_AKELA_FINAL_REPORT	
9. SPONSORING/MONITORING AGENCY NAME(S) AND ADDRESS(ES) ARMY RESEARCH OFFICE ARO 800 Park Office Drive Suite 4229 Triangle Research Park NC 27709				10. SPONSOR/MONITOR'S ACRONYM(S) ARO	
				11. SPONSOR/MONITOR'S REPORT NUMBER(S)	
12. DISTRIBUTION/AVAILABILITY STATEMENT Approved for public release; distribution unlimited					
13. SUPPLEMENTARY NOTES					
14. ABSTRACT Technical report detailing the results of AKELA/Michigan Tech Research Institute (MTRI) team investigations into exploitation of induced vibratory responses in buried targets using GPR. Results show significant improvement in SCR possible using these techniques. Range-Doppler filtering is presented along with enhanced SAR imagery in a laboratory setting demonstrating feasibility of GPR enhancement. Full wave simulations are used to bound performance expectations along with a detailed non-linear classification scheme based on cyclostationarity and dynamic mode analysis.					
15. SUBJECT TERMS Radar, GPR, multi-modal collection, vibration analysis, EHD					
16. SECURITY CLASSIFICATION OF:			17. LIMITATION OF ABSTRACT	18. NUMBER OF PAGES	19a. NAME OF RESPONSIBLE PERSON
a. REPORT	b. ABSTRACT	c. THIS PAGE			David Boutte
Unclassified	Unclassified	Unclassified			19b. TELEPHONE NUMBER (Include area code) 805-683-6414



Acoustically/Vibrationally Enhanced High Frequency Electromagnetic Detector for Buried Landmines

**Final Report for
W911NF-16-P-0013**

**Date
15 March 2016**

David Boutte, Vincent Radzicki,

**AKELA, Inc
5551 Ekwill Street, Suite A
Santa Barbara, CA 93111
dboutte@akelainc.com**

Adam Webb, Brian Thelen and Joseph Burns

**Michigan Tech Research Institute
Michigan Technological University
3600 Green Ct., Ste. 100
Ann Arbor, MI 48105
joseph.burns@mtu.edu**



TABLE OF FIGURES	3
INTRODUCTION AND PROBLEM STATEMENT	5
EXPERIMENTATION AND DATA ACQUISITION SYSTEM	5
ANALYSIS	8
Measurement of Vibrations through Radar	9
Differentiating Targets from Vibratory Signatures	15
Explosive Hazard Characterization and Identification from Acoustic Resonance Response	17
SIMULATION AND CYCLOLSTATIONARY ALGORITHMS	21
VIBRATION SIGNAL MODEL AND DETECTION ALGORITHM APPROACHES	26
Case 1: Collection of reference (non-vibrating) signal.	27
Case 2: Do not have reference (non-vibrating) image.	28
Dynamic Mode Decomposition	29
REFERENCES	32

Table of figures

Figure 1 AKELA Radar Sensor Unit (a.) and experiment apparatus (b.)	6
Figure 2 Surrogate EXH targets used in this research program	7
Figure 3 Aura NSW2 Loud-speaker (a.) and its frequency response (b.)	8
Figure 4 Block diagram of experimental radar/acoustic sensor system	8
Figure 5 Spring suspended metallic plate (a.) and target being buried underground (b.)	9
Figure 6 Range-Doppler map collected at a single aperture position of vibrating plate	10
Figure 7 Raw and filtered range profiles of vibrating plate	11
Figure 8 Acceleration data of metallic plate collected from independent accelerometer sensor.....	11
Figure 9 Spectrogram from SAR data of stationary plate (a.) and vibrating plate (b.)	12
Figure 10 FIR filter response used to extract harmonic signal from radar data	13
Figure 11 Raw waterfall plot (a.) and filtered waterfall plot (b.) of SAR data collected on vibrating plate	14
Figure 12 Experimental setup (a.) diagram (b.) unfiltered image reconstruction (c.) and the filtered image reconstruction (d.) of a vibrating plate.....	15
Figure 13 Subsurface clutter mitigation tests with (a.) test configurations, (b.) experimental data collection system (c.) raw B-scan and (d.) vibrating plate signature.....	16
Figure 14 Subsurface mine characterization experiments.....	17
Figure 15 Range profiles of stationary (a.) and vibrating (b.) 155mm artillery shell.....	18
Figure 16 Range profiles of stationary (a.) and vibrating (b.) M20 landmine.....	18
Figure 17 M20 landmine resonance detection test.....	19
Figure 18 M20 landmine resonance detection test B-Scans with (a.) raw data and (b.) resonant filtered data.....	19
Figure 19 Multiple target discrimination test.....	20
Figure 20 Multiple target discrimination test with (a.) raw B-scan and (b.) resonant detection response	21
Figure 21. A vibro-acoustic model is constructed to characterize the response to a localized pressure source applied to the ground layer.	21



Figure 22. The motion of the scene in response to the pressure excitation is shown on the surface (left), through the magnitude of the ground surface velocity, and the target (right) through the magnitude of the displacement vector. 21

Figure 23. The magnitude and phase of the y-component of the displacement as a function of frequency is compared for the buried target and a point on the surface directly above the buried target. 22

Figure 24 The y-component of the displacement as a function of time is compared for the buried target (left) and a point on the surface directly above the buried target..... 23

Figure 25 The frequency response of the z-component of the displacement is shown for the buried target and the surface..... 24

Figure 26. A small peak in the z-component of the amplitude response can be seen corresponding to the delay between the location of the excitation and the target. 24

Figure 27. The magnitude of the displacement oscillations is higher at the lower end of the frequency band. 24

Figure 28. (a) shows the spectrum of above ground vibrating plate, (b) the below ground vibrating plate. 30

Figure 29 (a) shows the eigenvalues of the vibrating plate on the surface, (b) shows the eigenvalues of the buried plate. 31



Introduction and Problem Statement

Development of remote sensing technologies that can accurately and reliably detect and classify explosive hazard (EXH) threats such as buried landmines and improvised explosive devices (IEDs) remains a critically important endeavor. The variety of EXH threats encountered in terms of size, material composition, camouflaging, and other factors pose many difficult technical problems, limiting the rate of progress in this field. Radar sensors have emerged as popular tool for this problem, given their ability to detect objects below ground and through optically opaque materials. Radar detection of EXH threats still face other issues, such as weak radar scattering from targets, spatial resolvability, and large amounts of reflecting clutter. Classification techniques and methodologies of EXH targets using radar sensors require mitigating these effects that drastically reduce the overall signal-to-noise ratio.

Classical radar systems will compute reflectivity maps, or images, of surveyed areas and from this classification algorithms will try to estimate the position and class of any EXH threats in the scene. As stated, this method tends to be susceptible to high clutter reflections and small scattering targets. To yield a higher signal-to-noise ratio for EXH targets, it would be beneficial to measure an additional physical parameter beyond reflectivity. For example, if the system could measure the vibratory resonance of an object while under excitation from an external acoustic source this could be used to discriminate objects with known shape and size from a building or wall. Radar systems that can measure motion, or Doppler, of targets can potentially also measure vibration in the form of micro-doppler [1][2][3].

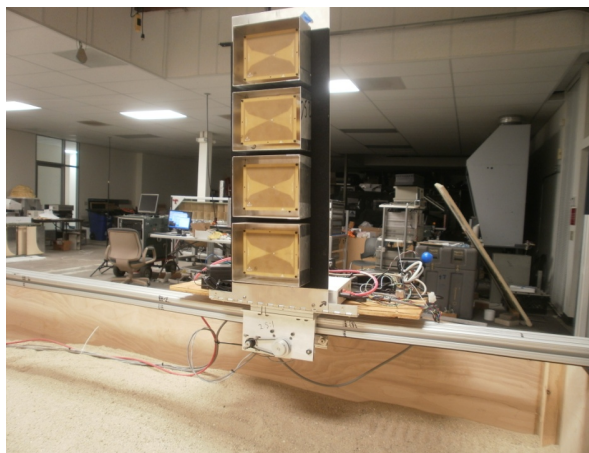
The research and development conducted to evaluate the performance gains of acoustically coupling vibration energy into EXH targets for radar sensing detection and classification is presented here. A prototype acoustic excitation and radar measurement unit was developed and utilized to measure experimental data on surrogate EXH targets. A test apparatus similar to the likely field environment was used for all data collection experiments to ensure realistic data.

Experimentation and Data Acquisition System

Close experimental validation was performed in conjunction with the system development for this research program. Careful measurements were carried out in an incremental fashion exploring the phenomenology of the problem while determining the performance limitations of the measurement systems. After a firm understanding of the phenomenology was established, surrogate EXH targets were measured and the ultimate detection performance gains that could be expected for such targets were determined.

The radar hardware system used for all data collection consisted of three main units: a two-port AKELA RF Vector Measurement Unit (AVMU), a linear antenna array, and a personal computer to control and program all the devices. The radar unit was completely programmable and

operated in the stepped-FMCW mode. The transmission signal parameters such as the frequency hopping rate, bandwidth, and frequency resolution are all user defined. The transmit power is approximately 50mW, and the operating frequency range chosen was 0.9GHz to 2.9GHz with 201 points for a total bandwidth of 1.1GHz. The frequency hopping rate was programmed up to 90,000 hops per second. The radar system was configured in a synthetic aperture spotlight mode to generate high resolution radar images of targets. To achieve the SAR scan, the entire radar array was mounted to an electronically controlled motorized rail system that would track position as the radar array moves. The entire radar system mounted to the rail above the test apparatus can be seen in Figure 1.



(a.)



(b.)

Figure 1 AKELA Radar Sensor Unit (a.) and experiment apparatus (b.)

The test apparatus consisted of an 8 ft. x 8ft. sandbox filled with homogenous dry sand with a dielectric constant of approximately 4. For most experiments the antennas pointed directly down at the sandbox which produces a large ground reflection that typically impacts detection performance. The surrogate targets of interest were measured both above the sand and in certain scenarios buried beneath the surface. This test apparatus allowed for consistent data quality and comparable experiments due to similar background environments. With the desired application of this research program in mind, a set of test targets were aggregated to measure and characterize. Firstly, a canonical radar target was constructed comprising of a flat metal plate suspended to a wooden frame via four springs. The spring suspension was designed so that vibration motion of the metal plate could be easily excited and thus serve as an optimal vibrating target. For a more realistic set of targets, a set of stimulant EXH mines were chosen and subsequently tested. The test targets utilized throughout the research study can be seen in Figure 2.



(a.) 155mm Artillery Shell



(b.) M20 Landmine



(c.) VS 2.2 Landmine



(d.) M19 Landmine

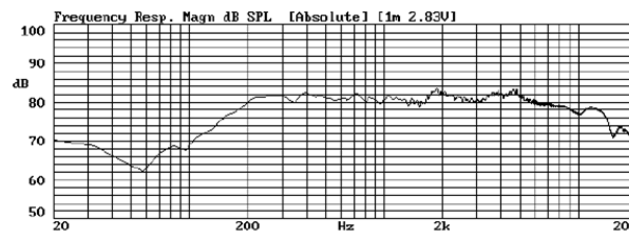
Figure 2 Surrogate EXH targets used in this research program

In addition to the radar measurement system, an acoustic source that could potentially excite targets with sufficient energy was required. For this task, the AURA NSW2 a high power low-frequency loud-speaker was utilized. The device and its frequency response can be seen in Figure 3. This device was driven by a current amplifier at low audio frequencies to yield large vibrational displacement of targets under test. For most experiments these devices were buried underground, so that the acoustic waves could propagate and induce motion in the test targets. To understand the acoustical coupling and vibration behavior of the environment and targets, additional motion sensors were employed. A geo-phone (SM24-UB) and accelerometer (ADXL103) were selected for this task. The geo-phones were typically buried to measure the local acoustic vibrations of the sand, and the accelerometer was fixated to targets to measure their vibration.



(a.)

Frequency Response (1W, 1m)



(b.)

Figure 3 Aura NSW2 Loud-speaker (a.) and its frequency response (b.)

During the data collection experiments, the sensor systems were instrumented to measure the various physical parameters of interest including target vibration, seismic vibration, radar signal reflections, and antennas’ positions. The sensor instruments and radar system were all controlled through a single computer for synchronization and further post-processing. A block diagram outlining the high-level measurement system is shown in Figure 5. With the measurement system configured as shown, all the various physical variables could be measured and compared to the radar detection performance so as to establish the requisite conditions and radar design parameters.

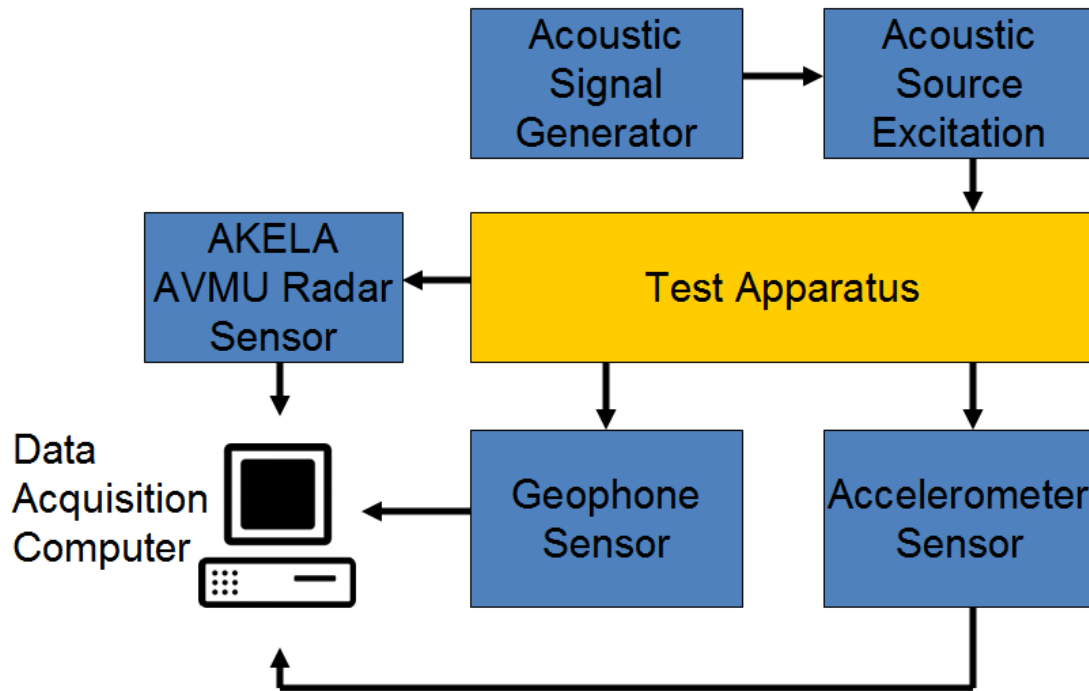


Figure 4 Block diagram of experimental radar/acoustic sensor system

Analysis

A sequence of experiments studying the key issues of this research program was designed, executed, and the appropriate conclusions were drawn. Firstly, the performance limitations of the radar system’s ability to measure vibratory targets were established. Here, a few operating specifications such as signal-to-noise ratio and measurement sensitivity were determined and the feasibility of target detection was analyzed. Following this basic verification, more advanced testing was conducted to localize vibration targets as well as differentiate them from stationary clutter. Using these results, a final series of experiments were carried out to measure the



detection performance on surrogate EXH targets and verify the feasibility of the proposed methodology.

Measurement of Vibrations through Radar

The initial vibration testing with the radar system mainly focused on the spring suspended metal plate. The surrogate vibrating target was excited to vibrate in a periodic manner by attaching a small motor to its face that would rotate at a fixed frequency, thus inducing a proportional vibration. The target was instrumented with an accelerometer sensor and enclosed by non-reflective foam so that it could be buried during data collection experiments. The target was first measured directly below the transceiver array buried approximately 3in. in the sand, as can be seen in Figure 5. The plate was excited using a motor with an offset weight to vibrate at an oscillation frequency of approximately 20Hz. A time-sequence of range profiles was measured with the radar array in a stationary position while sampling fast enough to avoid aliasing. The Range-Doppler map of those measurements was processed and can be seen in Figure 6. The majority of the energy in the scene is concentrated around the zero-Doppler bins as would be expected given a stationary scene and target. However, a large peak in spectral energy is evident around 20Hz and at the correct range of the target and corresponds to the correct rate of vibration.



(a.)



(b.)

Figure 5 Spring suspended metallic plate (a.) and target being buried underground (b.)

The target was first measured directly below the transceiver array. The plate was excited using a motor with an offset weight to vibrate at an oscillation frequency of approximately 20Hz. A time-sequence of range profiles was measured with the GPR array in a stationary position while sampling fast enough to avoid aliasing. The Range-Doppler map of those measurements was processed and can be seen in Figure 6. The majority of the energy in the scene is concentrated around the zero-Doppler bins as would be expected given a stationary scene and target.

However, a large peak in spectral energy is evident around 22Hz and at the correct range of the target which corresponds to the correct rate of vibration for the target.

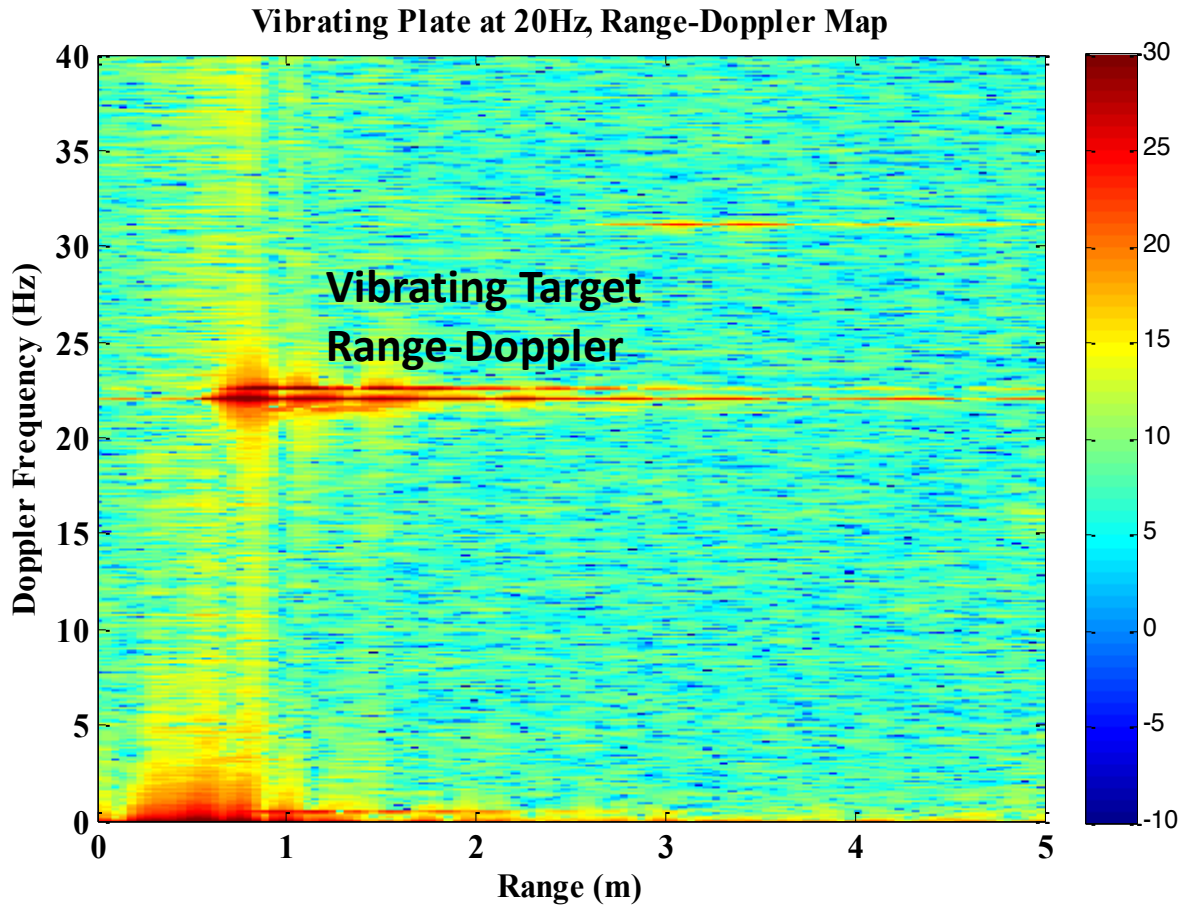


Figure 6 Range-Doppler map collected at a single aperture position of vibrating plate

The range-profile corresponding to the highest non-zero Doppler peak was extracted and compared to a raw range-profile of the target as plotted in Figure 7. The unprocessed range profile includes numerous peaks from many clutter objects including the antenna-leakage, ground reflection and others. Filtering out the non-zero Doppler peak at the equivalent rate of vibration of the target, however, yields a single large peak at the range of the target, with the surface reflection and antenna leakage attenuated by more than $50dB$. As can be seen the target peak falls in magnitude due to the loss of the DC term, however, the significant drop in clutter energy would produce a greater signal-to-clutter peak, and thus greater probability of detection and more intuitive analysis.

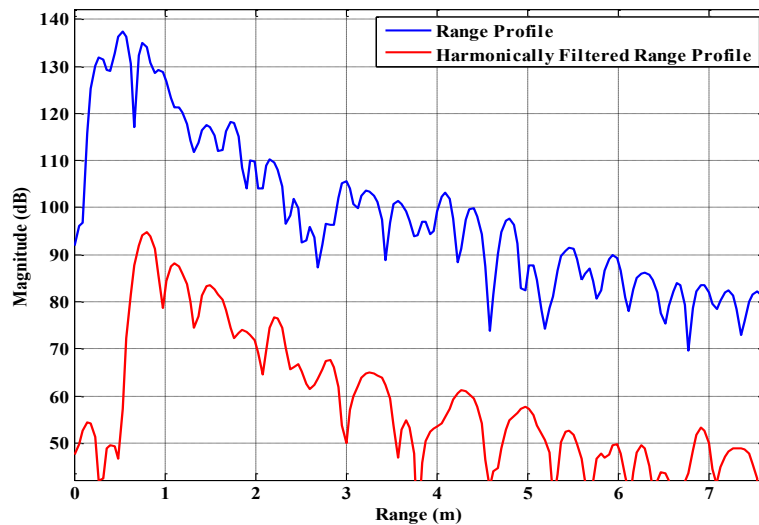


Figure 7 Raw and filtered range profiles of vibrating plate

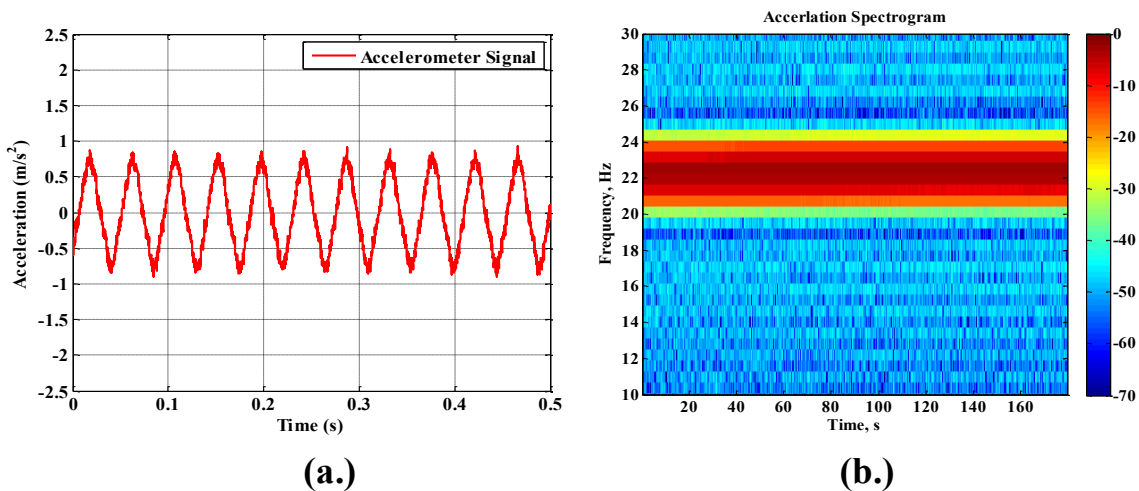


Figure 8 Acceleration data of metallic plate collected from independent accelerometer sensor

To verify the vibration frequency estimation results of the radar system an accelerometer was also employed to measure the vibration frequency. The accelerometer was attached directly to the vibrating surface of the plate and would correspond to the range vibration seen by the radar sensor. The acceleration data was collected concurrently to radar data collection and then analyzed using a Short-Time Fourier Transform (STFT) to estimate its rate of vibration. The analysis can be seen in Figure 8, where the large peak at 22Hz matches very closely to the radar estimate as well. This correspondence of estimates between two different sensor modalities,

demonstrates that the radar system employed can both estimate the frequency of targets vibrating in range as well as use that estimate to discriminate among different targets.

The system and vibrating plate target was next tested in the desired SAR mode, so that cross-range information target localization can be achieved. In this configuration, the target was buried in the center of the sandbox. The radar array was then scanned from one end of the sandbox to the other passing directly over the target. A STFT result of a single CW-measurement was produced to determine if the vibration signal was being over-damped by the array motion. Figure 9 compares the STFT results of the vibrating target and non-vibrating target to demonstrate, that in fact the periodicity of the target motion can still be captured in SAR mode. The rate of vibration is measured only when the vibrating target comes directly into view of the radar sensor, however, a small frequency modulation component is induced from the relative motion of the SAR with respect to the target.

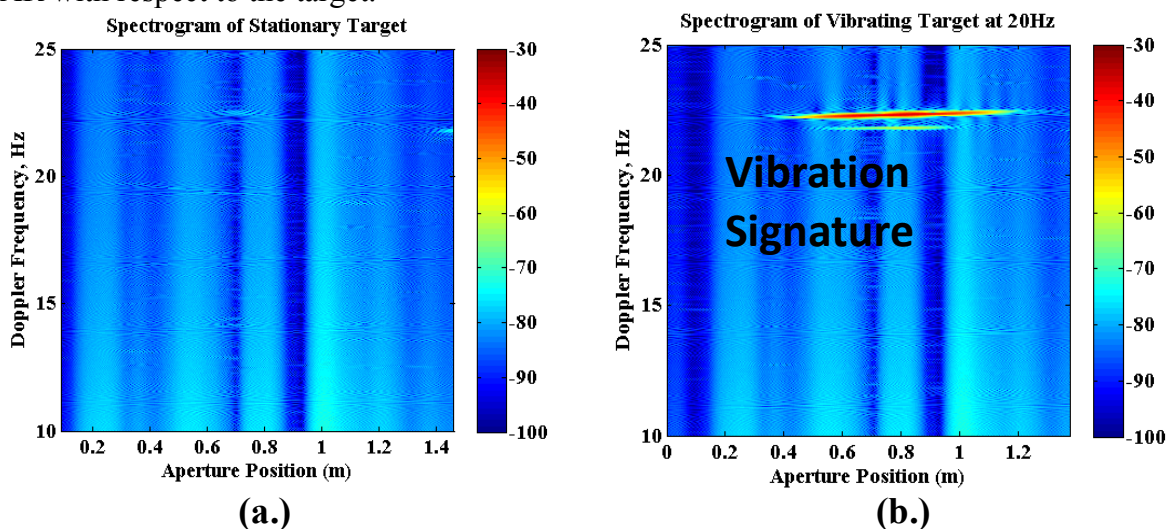


Figure 9 Spectrogram from SAR data of stationary plate (a.) and vibrating plate (b.)

A full FMCW sweep was also measured of the vibrating target in SAR mode so that ranging and cross-range information could be inferred and the target image could be reconstructed. Exploiting the information that the vibrating target’s range information resides in the frequency band proportional to its rate of vibration, and the clutter is mostly at zero-doppler the SAR data was appropriately filtered for the known target vibration frequency. The SAR data was processed over scan position using an FIR filter to preserve the phase information of the frequency data while filtering out all the non-resonance motion in the scene. The filter response can be seen in Figure 10, and as can be seen was centered on the expected rate of vibration of 22Hz with approximately 10Hz bandwidth.

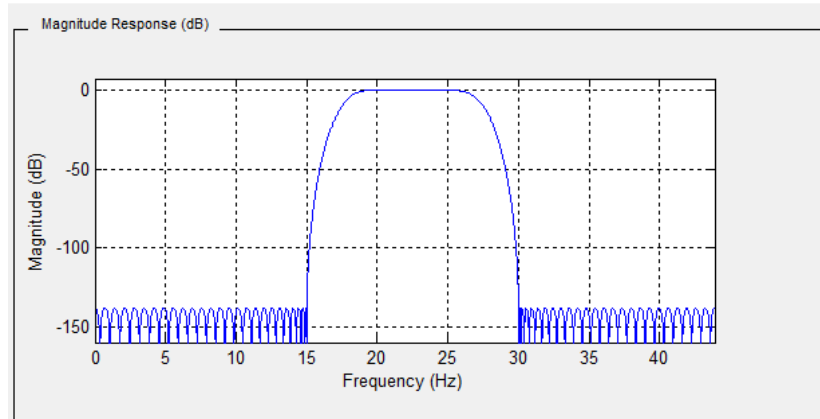


Figure 10 FIR filter response used to extract harmonic signal from radar data

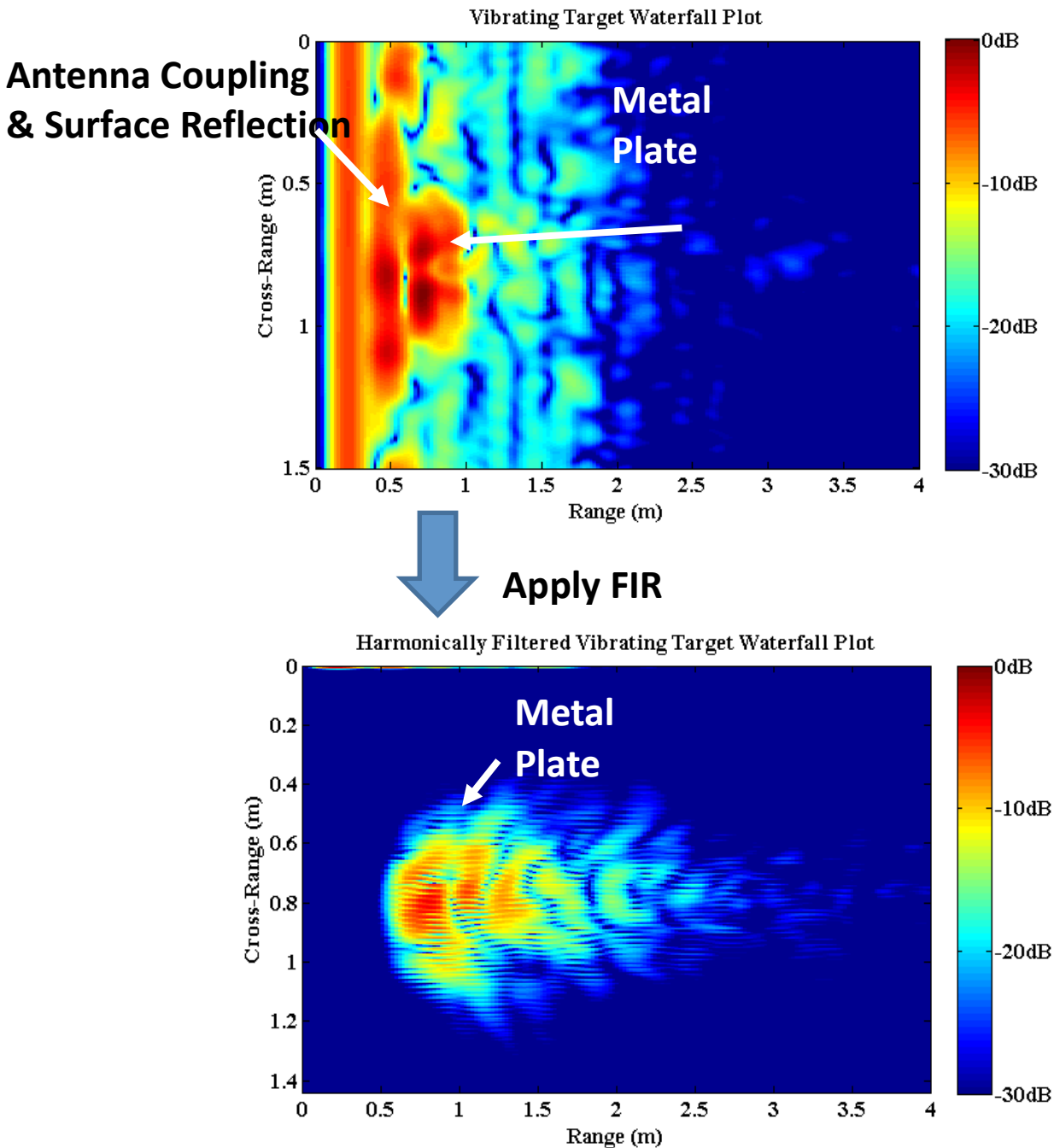


Figure 11 Raw waterfall plot (a.) and filtered waterfall plot (b.) of SAR data collected on vibrating plate

Two B-scans of the unfiltered SAR data and after the FIR filtering is displayed in Figure 11. Here the clutter mitigation effects are very pronounced as the antenna coupling and surface reflection are greatly reduced. There exists some artifacts from the filtering, however, including secondary range peaks potentially due to multiple reflections of the environment as well as target

scintillation effects. These artifacts will introduce some duration in the final image quality; however, the clutter mitigation gain would outweigh typical losses. Performing a full back-projection image reconstruction from the B-scans was done, and the results of which are seen in Figure 12. The reduced clutter in the raw image compared to the filtered image is around 5-10dB. Although, the FIR filtering produces greater levels of specular noise in the final image, the large clutter targets have been greatly mitigate which can help improve target detection and classification tasks greatly.

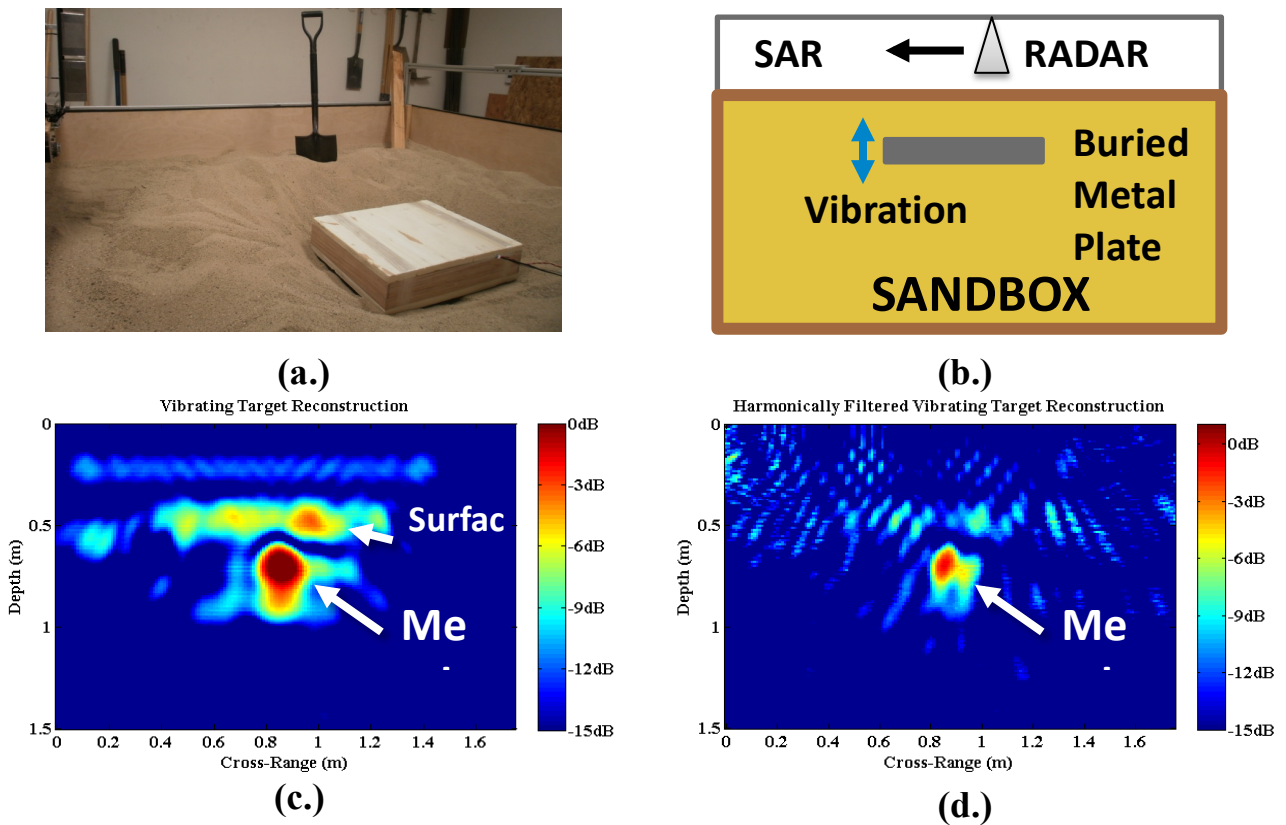


Figure 12 Experimental setup (a.) diagram (b.) unfiltered image reconstruction (c.) and the filtered image reconstruction (d.) of a vibrating plate

Differentiating Targets from Vibratory Signatures

Beyond mitigating stationary clutter, Doppler extraction of vibrating targets may also serve as a feature that can characterize and identify specific targets from other superfluous clutter based on vibration signatures. Further, experimentation and analysis was conducted to explore and exploit this idea. The vibrating metal plate target was again buried and measured utilizing a SAR scan with the radar sensor while vibrating. To simulate clutter that is typically encountered while performing subsurface radar imaging, two metallic structures were also buried. A copper corner reflector and a secondary metallic plate were both buried during data collection.

Because the vibrating plate contains a different vibratory signature than the stationary clutter, spectrally filtering the range-Doppler targets at specific vibration frequencies of interest would remove the stationary buried targets from the measured scan. The experimental configuration for this approach can be seen in Figures 13a and 13b. The range-profiles were then displayed over the aperture position, to form a B-scan of the sub-surface profile. In the raw B-scan in Figure 13c, all three buried objects are visible due to their high radar reflectivity; however, it is not possible to determine which targets are vibrating or stationary. Spectrally filtering at the known vibration frequency of the metal plate drastically reduces the signal-to-clutter ratio by over 15dB as is seen in Figure 13d. This gain not only increases the probability of detection, but also produces a more intuitive image to analyze for non-technical users.

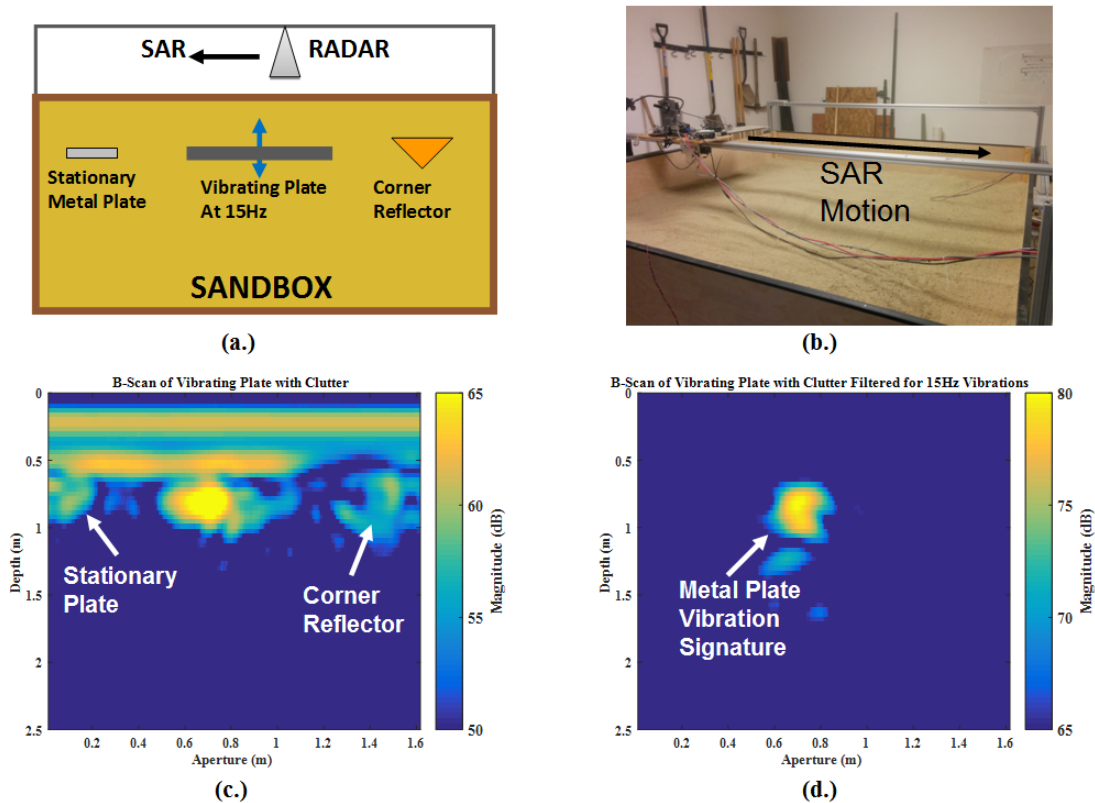


Figure 13 Subsurface clutter mitigation tests with (a.) test configurations, (b.) experimental data collection system (c.) raw B-scan and (d.) vibrating plate signature

Two advantages of target vibration estimation have been identified, the first being clutter mitigation and second target classification. If there are any targets present in a scanned radar data that are known to be vibrating at a certain frequency, this methodology can be utilized to greatly enhance the probability of detection and classification. If targets that are normally stationary, such as EXH devices, could be made to vibrate the methodology demonstrated here could also be used for detection and classification.

Explosive Hazard Characterization and Identification from Acoustic Resonance Response

With the basic methodologies for measuring and discriminating vibrating targets established, the next step was to characterize the vibratory spectral response of various targets to an external acoustic excitation. To measure this, the Aura NSW2 loud-speaker was buried approximately three inches in the sandbox and the target under test was placed directly above it. The geophone sensor was then set on the surface of the target to measure its vibration amplitude. The acoustic source was swept from 15Hz-150Hz for each of the surrogate EXH targets examined for this research program. The normalized spectral response of each surrogate target was calculated and then plotted in Figure 14. The response up to 50Hz is mainly dominated by the resonance of the acoustic source, however, the targets of higher mass do not vibrate as strongly. Beyond 50Hz, the response of the targets then begins to dominate. The responses of both the 155mm artillery shell and the M19 landmine die out past 75 Hz, yet the M20 landmine and VS 2.2 landmine begin vibrating more strongly until they approach their resonant frequencies.

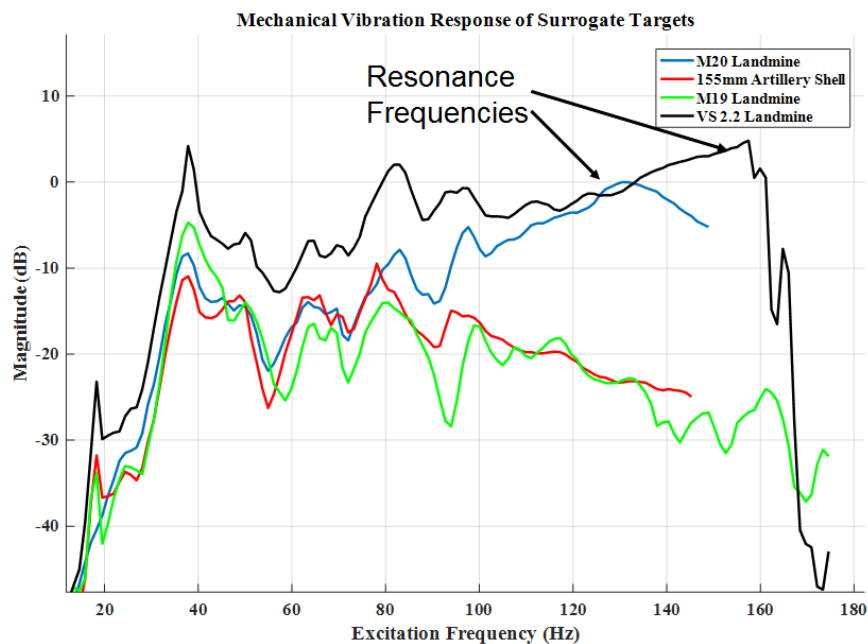


Figure 14 Subsurface mine characterization experiments

The difference in resonance frequencies among different targets can be exploited to perform classification and detection. Since one target will vibrate much stronger at resonance compared to another target, the resonant target will also have a much stronger vibratory signature in the radar measurement. To illustrate this idea, both the 155mm artillery shell and the M20 landmine



were excited at various acoustic frequencies and measured with the radar sensor simultaneously. Figure 15 demonstrates that 155mm artillery shell's range profile response is clearly visible up to 75Hz, however, past this begins to disappear beyond this as supported by Figure 14. The M20 landmine's range profile response is still very strong at 130Hz, its resonant response.

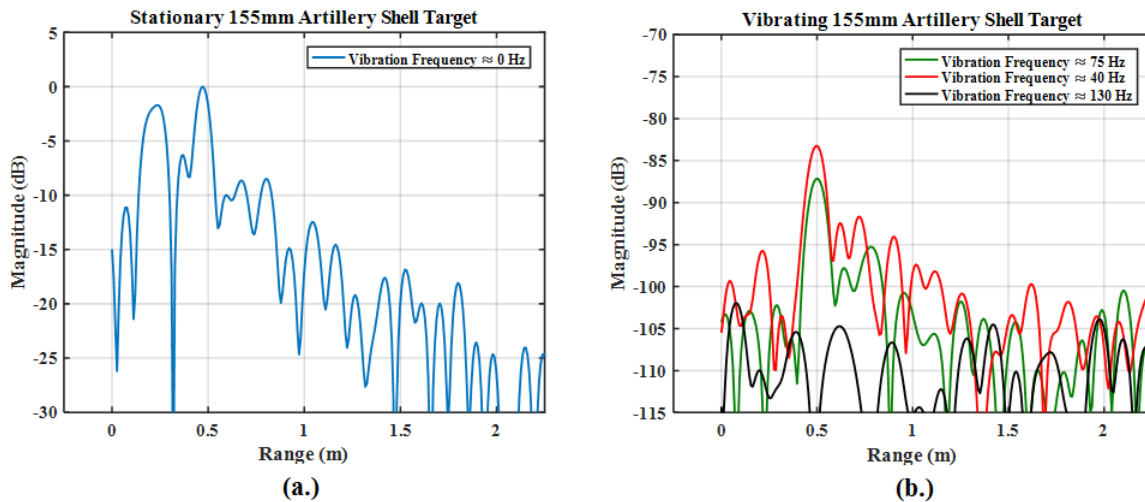


Figure 15 Range profiles of stationary (a.) and vibrating (b.) 155mm artillery shell

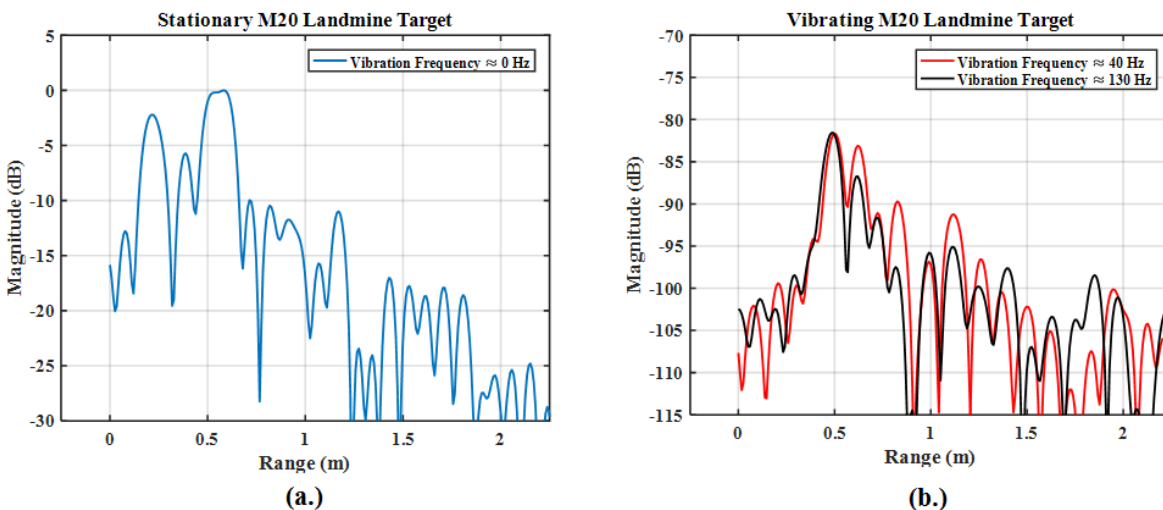


Figure 16 Range profiles of stationary (a.) and vibrating (b.) M20 landmine

To test the discriminatory capability of the resonant response, the M20 target was measured under a SAR scan surrounded by other clutter objects, as shown in Figure 17. The acoustic source was excited at the resonant frequency of the M20 during data collection, and the

subsequent radar sensor data was also filtered for this vibration frequency. The raw B-scan and spectrally filtered B-scan were computed and are plotted in Figure 18. Here again, in the raw B-scan all of the superfluous clutter components are visible at various magnitudes, and obfuscate the location of the M20-landmine. However, after filtering for the vibration signature of resonant target, the M20 is the by far the strongest visible component remaining in the B-scan. A small multi-path component resides below the main lobe of the target, however, the clutter objects again have been greatly mitigated.

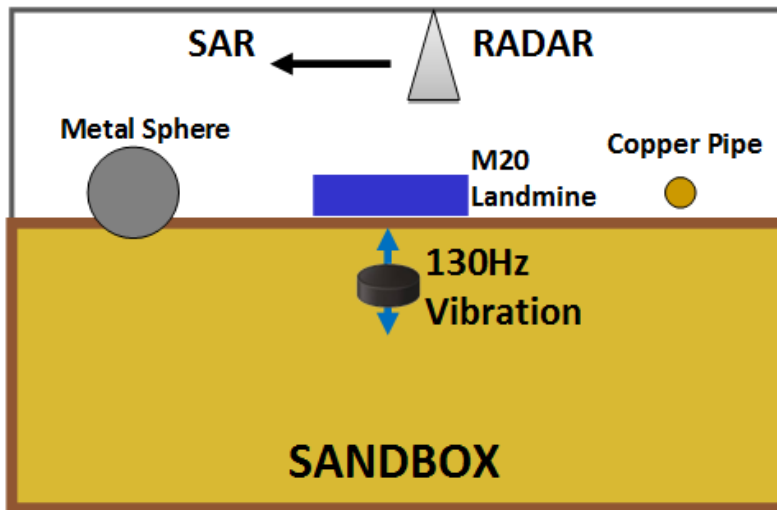


Figure 17 M20 landmine resonance detection test

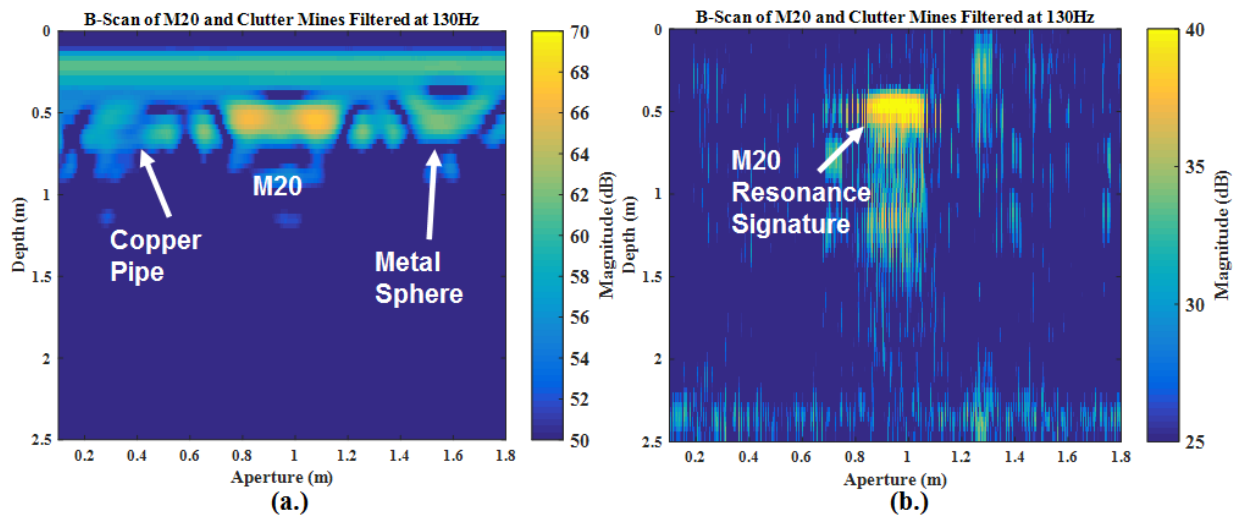


Figure 18 M20 landmine resonance detection test B-Scans with (a.) raw data and (b.) resonant filtered data

The resonant response for the M20 is strong enough to mitigate clutter, but it is also desirable to use resonant responses to discriminate among multiple EXH targets. A similar experiment was designed, where two surrogate targets the M20 landmine and the 155mm artillery shell were simultaneously measured again. As seen in Figure 19, two acoustic sources were placed directly below each target to simulate a uniform excitation from a remote source that would be utilized in a field scenario. Both targets were excited at the resonant frequency of the M20 landmine, to determine if the radar could discriminate between the targets. The subsequent B-scans before and after resonant filtering can be seen in Figure 20. As in the previous testing the clutter signatures are reduced dramatically, but now the non-resonant target is also filtered from the data.

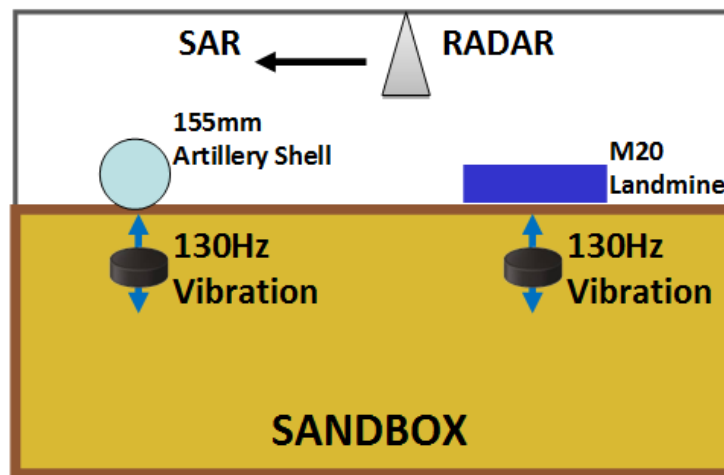


Figure 19 Multiple target discrimination test

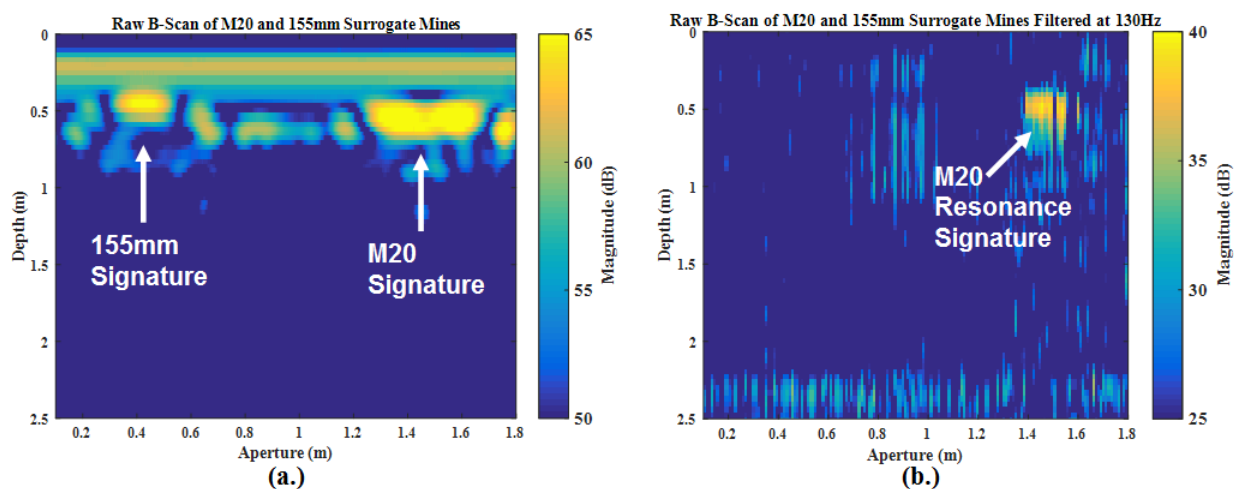


Figure 20 Multiple target discrimination test with (a.) raw B-scan and (b.) resonant detection response

The vibratory sensitivity of the radar system presented in this research has been demonstrated to be accurate enough not only to discriminate vibrating targets from stationary clutter, but also discriminate among multiple vibrating targets of differing acoustic responses. This high gain in signal-to-clutter ratio as well as strong discriminatory capabilities, signify that this technique could be very effective in field scenarios. The proposed methodologies have been tested against stimulant EXH devices and demonstrated that it can be effective against such threats in terms of detection as well as classification. The resonant filtered B-scan could directly be used with a CFAR threshold detector, or potentially more advanced time-frequency transformations could be utilized as well for the more robust classification algorithms. A key technical challenge that remains will be the design of acoustic sources that transfer enough vibration energy into potential targets. A good amount of research work has been performed on this problem for seismic imaging problems, which could be leveraged with the strong results presented here to yield a viable detection system that surpasses current technology.

Simulation and Cyclostationary Algorithms

One goal of the MTRI effort is to numerically simulate the vibrations of a target buried in the ground when the ground is acoustically or seismically excited by a localized pressure source. The predicted target vibrations can be used to assess their detectability using a standoff radar system. The hybrid acoustic/structural finite element method simulation performed for the phase I effort is summarized below.

The purpose of the simulation was to characterize the vibration of the ground, as well as the vibration of a buried target, when localized forces are applied to the ground surface. The numerical simulations were performed in the frequency domain using LMS Virtual Lab's vibro-acoustic finite element method solver.

In this framework, we constructed the representative model, shown in Figure 1, which had a ground medium with a 0.20 m^3 steel cube buried 3 cm beneath the surface. An excitation is provided by a 0.1 m^2 pressure source located approximately 0.75 m away from the buried target. The source was assigned a pressure level at each frequency which corresponded to the spectral response of a 40 kN impulse in the time-domain. The resulting vibration response was computed at 200 discrete frequencies sampled at 20 Hz increments ranging from 20 Hz to 4 kHz . Given the number of frequency samples and the size of the source, the appropriate pressure applied at each frequency sample was determined to be 20 kN/m^2 . The ground layer is modeled as an acoustic

fluid and energy is transferred through the fluid acoustically to the buried target. The structural response of the target to the acoustic field is then determined through the computational structural dynamics (CSD) solver included in the LMS environment.

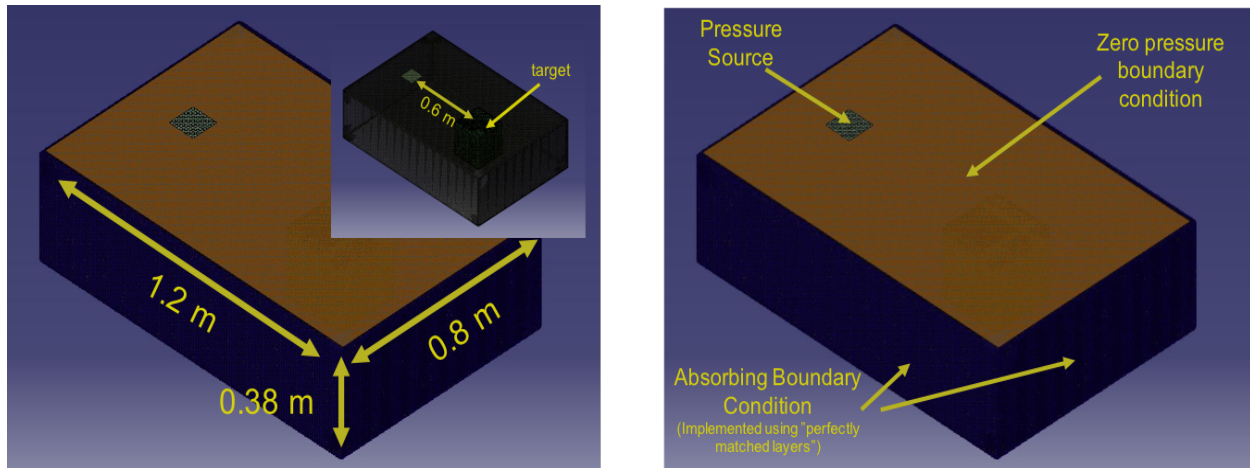


Figure 21. A vibro-acoustic model is constructed to characterize the response to a localized pressure source applied to the ground layer.

The finite extent of the simulation domain is bounded on the surface by a zero-pressure boundary condition allowing the surface to move freely in response to the applied pressure source. The remaining 5 bounding surfaces are assigned an absorbing boundary condition implemented through perfectly-matched-layers automatically generated by the LMS software. The perfectly-matched-layers are constructed using complex anisotropic materials designed specifically to absorb any and all acoustic energy thus creating a boundary condition representative of a ground medium of infinite extent.

The LMS software provides a variety of ways to visualize the simulation output. Two images are shown in **Error! Reference source not found.** characterizing the motion of the surface (left),

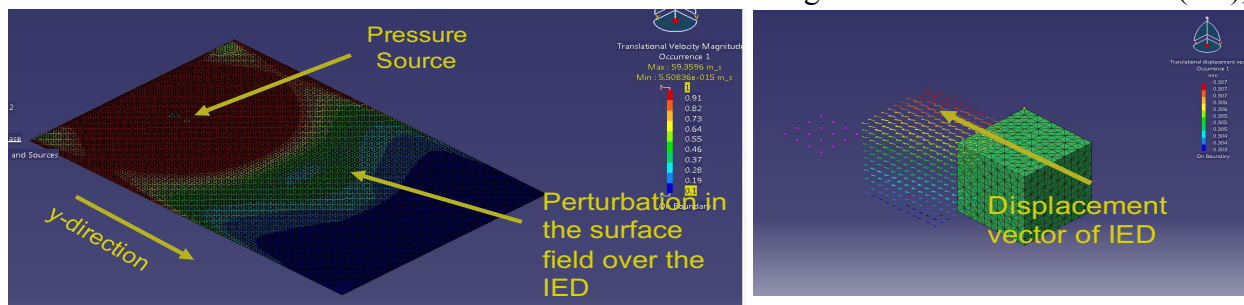


Figure 22. The motion of the scene in response to the pressure excitation is shown on the surface (left), through the magnitude of the ground surface velocity, and the target (right) through the magnitude of the displacement vector.

through the magnitude of the ground surface velocity, and the target (right) through the magnitude of the displacement vector. The surface velocity field shows a clear perturbation above the buried target.

The plots in **Error! Reference source not found.** and 4 compare the *y*-component of the displacement of the target with the surface displacement directly above the target. **Error! Reference source not found.** shows the magnitude and phase of the response as a function of frequency while 4 shows the real component of the displacement as a function of time. The time-domain response is computed through inverse Fourier transform of the frequency response and approximates the response to an impulse excitation occurring at $t = 0$. In this case, the *y*-

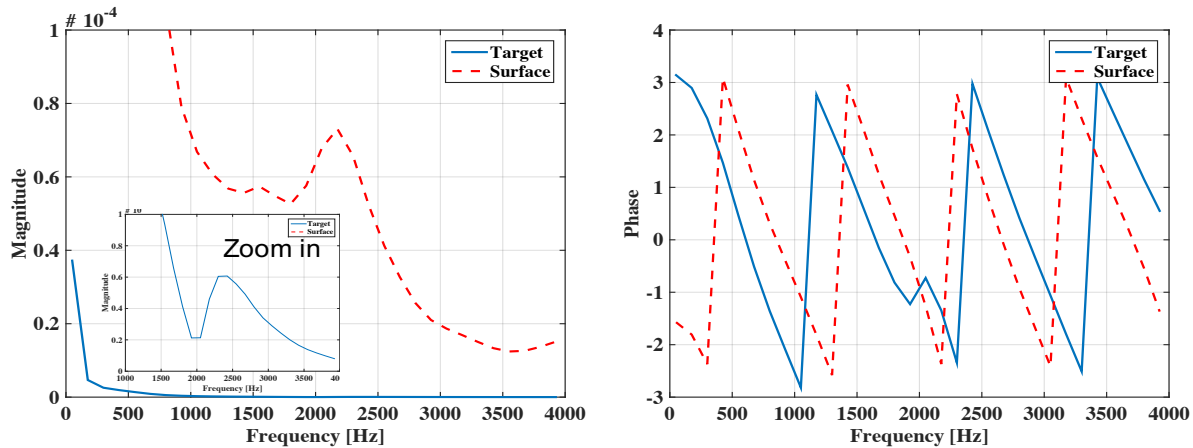


Figure 23. The magnitude and phase of the *y*-component of the displacement as a function of frequency is compared for the buried target and a point on the surface directly above the buried target.

component of the response in the model is clearly much stronger on the surface than the buried target. A peak in the target response is observed near 2400 Hz and similarly a peak in the surface response occurs near 2100 Hz. Given the speed of sound in soil, which was modeled to be 500 m/s, this corresponds to wavelengths of approximately 20 cm and 24 cm in the acoustic medium. It is believed that these resonances are created by the “waveguide” formed between the target and the surface given that the sides of the target cube are 20 cm in length. If you look closely at the time domain signals, the peak of the response at the surface and on the target occurs near $t = 1 \times 10^{-3} s$ but are slightly shifted due to the difference in range from the source to the analyzed point on the buried target and the analyzed point on the surface.

The frequency and time domain displacement plots are repeated in Figures 5 and **Error! Reference source not found.**, respectively, but this time characterizing the z-component of the displacement. In this case the magnitude of the response between surface and target are on the same order of magnitude but the difference in shape is more pronounced. A clear peak in the surface response is observed near 1400 Hz. In the acoustic ground this corresponds to a wavelength of approximately 36 cm. Given that the depth of the modeled ground region is 38 cm, it appears that this spike may be an artifact of the simulation caused by the finite extent of the ground. A small peak in the target response once again appears between 2000 and 2500 Hz due to the dimensions of the target. The peaks identified in the modeled responses have all been identified as resonances occurring in the acoustic ground. The speed of sound in solid steel is on the order of 6000 m/s. Given a highest modeled frequency of 4000 Hz this produces a

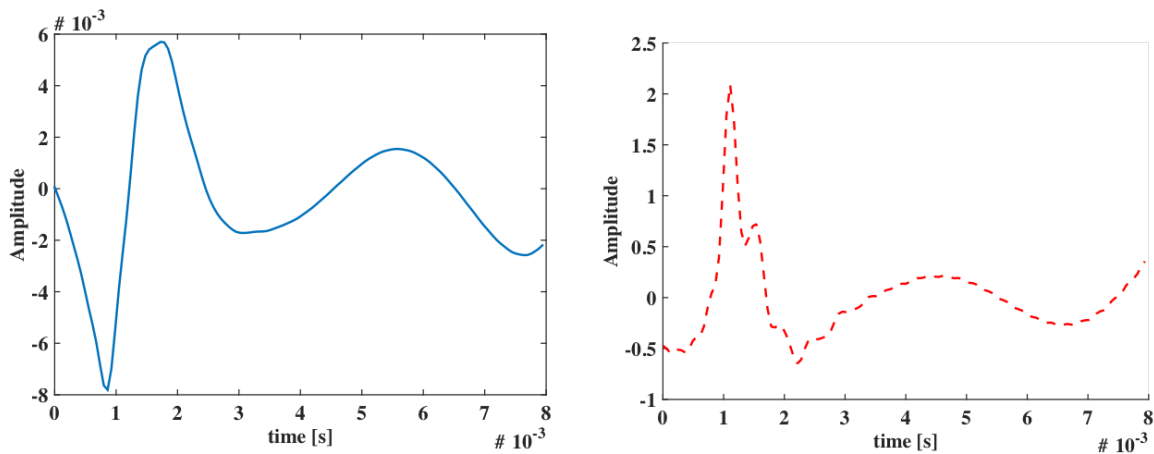
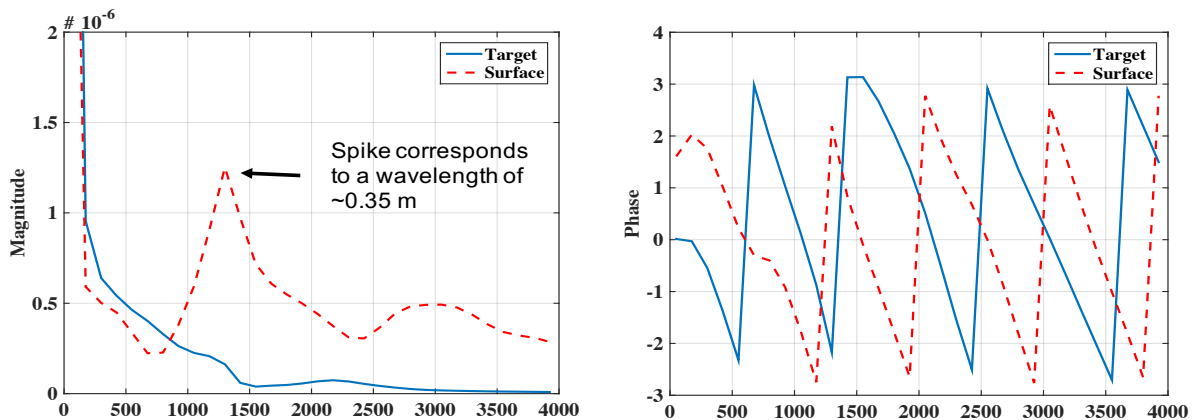


Figure 24 The y-component of the displacement as a function of time is compared for the buried target (left) and a point on the surface directly above the buried target right



wavelength of 1.5 m, thus for this low-bandwidth

Figure 25 The frequency response of the z-component of the displacement is shown for the buried target and the surface

approximation of an impulse no resonances in the target are expected.

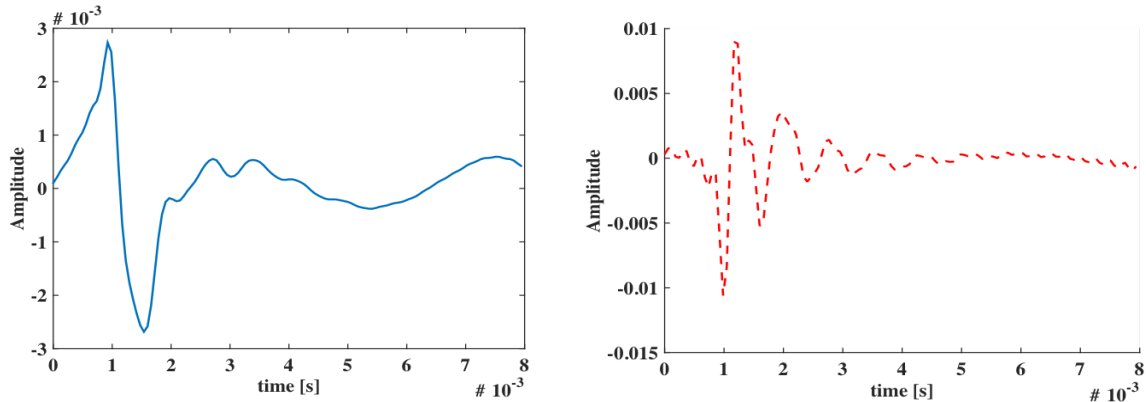


Figure 26. A small peak in the z-component of the amplitude response can be seen corresponding to the delay between the location of the excitation and the target.

Perhaps some comments are in order regarding the low amplitude of the simulated fluctuations in the time-domain. In these simulations, the force was spread out across a large bandwidth in the frequency domain to obtain a rough approximation to an impulse (time-domain) excitation. In reality, the amplitude of the displacements is larger for lower frequency excitations. As a demonstration of this we perform a second simulation spreading out the 40 kN force over only 10 frequency samples ranging from 10 to 100 Hz. The magnitude of the displacements in the frequency domain for the y- and z- components are shown in **Error! Reference source not found.**. These results translate to displacements on the order of *cm*'s for the y-component and *mm*'s for the z-component.

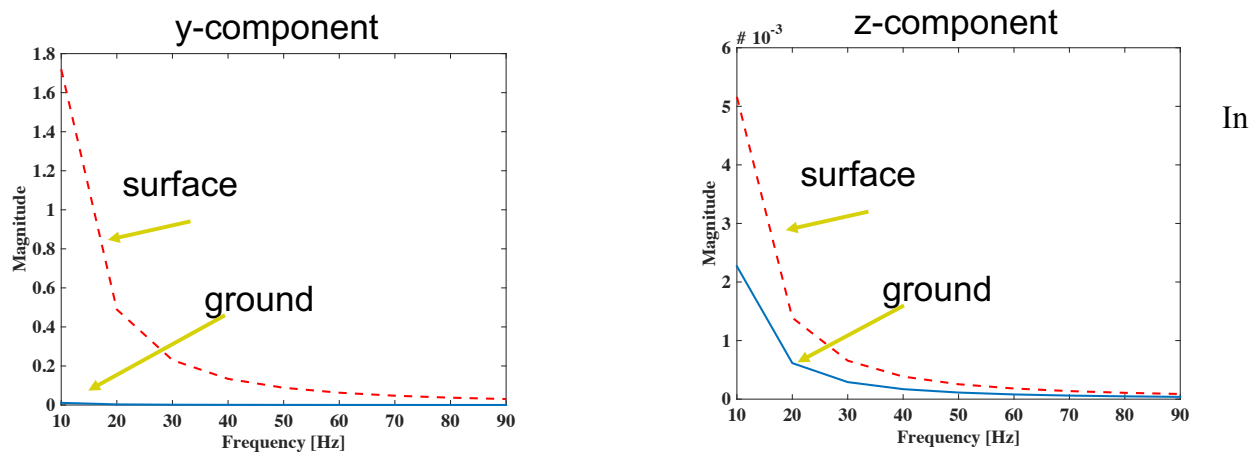


Figure 27. The magnitude of the displacement oscillations is higher at the lower end of the frequency band.

summary, an approach to numerically simulating the vibration of a buried target and surrounding surface in response to a localized pressure excitation of the surface was demonstrated. The resulting examples, showed vibrations with amplitudes that are potentially observable by radar sensors. The works shows that the Akela/MTRI team has a numerical method of exploring the vibrational response of buried targets for system design and analysis.

Vibration Signal Model and Detection Algorithm Approaches

Algorithmic approaches for both detecting and classifying buried target vibration signatures are presented. These algorithms can provide a basis for developing and evaluating a signal-processing framework for the system in Phase II. The model for the return at pulse time t is given as

$$s(x; t) = \rho_t * \sigma(x; t) + n(x; t)$$

where x is the = 1D/2D-spatial location depending on whether stationary or moving, t is the slow/pulse time, ρ_t is the so-called point-spread function (PSF) of the system at time t , and $\sigma(x; t)$ is the reflectivity at location x and time t and $n(x; t)$ is the noise. We utilize an index of t on the correlation ρ_t to account for any natural evolutions of the signal over “slow” time, which must be accounted for. This will be discussed in a little more detail, later in this section.

Now in the case of vibration, the main effect is a displacement in x at time t , which can be represented as

$$\sigma(x; t) = \sigma(x + v(x; t))$$

where $v(x; t)$ is actual displacement at time t . Now the model for the vibration is that there is a vibration-inducing waveform $w(t)$ whose Fourier transform is $W(f)$. We assume that there is a spatial transfer $\Gamma(x; f)$ so that the resultant frequency content from location x is $V(x; f) = \Gamma(x; f)W(f)$, the frequency representation of $v(x; t)$. Utilizing this model allows a natural means to consider what are good waveforms to transmit – specifically, it will be those that allow us to detect unique target vibrational signature in the presence background ground vibrational signatures. This will be discussed in a little more detail later in this section.

Based on this model, and assuming a single tone or a reasonably narrow-to-moderate bandwidth waveform, we have that

$$\sigma(x; t) = \sigma(x) e^{ih(x; t)}$$

where

$$h(x; t) = \frac{v(x; t)}{2\lambda}$$

with λ being the center wavelength. Since the vibrations are typically small relative to a wavelength,

$$\sigma(x; t) \approx \sigma(x)(1 + ih(x; t)) = \sigma(x) + i\sigma(x)h(x; t)$$

and so the model becomes that of

$$\begin{aligned} s(x; t) &= \rho_t * \sigma(x) + i\rho_t * (\sigma(x)h(x; t)) + n(x; t) \\ &= s_1(x; t) + s_2(x, t) + n(x; t) \end{aligned}$$

i.e., we get the original image without vibration plus a piece that is due to the vibration. Now we assume for simplicity that at some local spatial scale, we have a rigid body and everything locally (relative to resolution) is vibrating in the same way.

Now the main claim is that the spatial pattern of the vibration is different between when there is only ground vs. when there is ground with a target. Thus we are doing a hypothesis testing problem based on the data along the lines of

$$H_0: h(x; t) = h_{grd}(x; t) \quad \text{all } x$$

vs.

$$H_1: h(x; t) = \begin{cases} h_{grd}(x; t) & x \in \mathcal{X}_{\overline{targ}} \\ h_{grd}(x; t) + h_{targ}(x; t) & x \in \mathcal{X}_{targ} \end{cases}$$

Now there are two approaches to this – one is a total model-based approach for the vibrations, which says that we know what vibrational models hold for the ground and the target, and you fundamentally utilize those in terms in detection.

We consider two cases, one in which we first collect a data set without any vibration, and then a second in which we only collect data with vibration. The key concept for the first case is that this scenario allows us to see the first term of the signal model, and utilize that to carry out a careful analysis on what is the additional vibrational signature component, and do detection for target-induced anomaly.

Case 1: Collection of reference (non-vibrating) signal.

Here we present a high-level approach for utilizing this powerful additional information, and significant details would be needed to see how sensitive/valid this proposed approach could be in practice. The main advantage of this approach is that it can rigorously take into account inhomogeneous properties of the ground and isolate those from the vibration movements of the ground. The basic steps of this algorithm are:

Step 1: Estimate $s_1(x; t)$ as $\hat{s}_1(x; t)$

Step 2: Subtract of to get

$$s(x; t) - \hat{s}_1(x; t) \approx s_2(x; t) + n(x; t)$$

Step 3: Apply filtering operation to generate estimate of estimate of $h(x; t)$ – specifically, note that

$$\mathcal{F}s_2(x; t) = i\mathcal{F}\rho_t\mathcal{F}(\sigma \cdot h_t) = i\mathcal{F}\rho_t \cdot (\mathcal{F}\sigma * \mathcal{F}h_t)$$

and so can do some soft-filtering/division of

$$\frac{\mathcal{F}s_2(x; t)}{i\mathcal{F}\rho_t} = \mathcal{F}\sigma * \mathcal{F}h_t$$

and then do a deconvolution with $\mathcal{F}\sigma$ to obtain $\mathcal{F}h_t$. Note that we can utilize a finer-resolution version of σ for this since we can use the whole time-history. These estimated $\hat{h}_t(x)$ can then be processed to assess spatially utilizing CFAR type of analysis and cyclic spectral density hypothesis testing to determine whether there is a target vs. clutter type of vibration occurring.

Case 2: Do not have reference (non-vibrating) image.

In this case we are assuming a sort of regularity or some sort of homogeneity in terms of the vibrational patterns on the surface – this may not be strictly true as we have shown in the analysis section, that the resultant signature does depend on the underlying reflectivity of the ground.

Step 1: In this case, carry out a cyclic-spectral density estimation, that is space-localized in x , i.e., generating

$$\tilde{\mathcal{S}}_S(x) = \{\mathcal{S}_S(x; \alpha; w); (\alpha, w) \in A_F\}$$

Step 2: Generate mean/covariance statistics (stationary in x) in the CFAR region centered at x , i.e., generate mean and covariance of $\{\tilde{\mathcal{S}}_S(x'); x' \in N_{CFAR}(x)\}$ – this will correspond to null hypothesis means and covariance assuming no target. Denote mean and covariance as $\mu_o(x)$ and $\Sigma_o(x)$ for the vector $\tilde{\mathcal{S}}_S(x)$

Step 3: Generate optional alternative mean and/or covariance statistics in the CFAR region based on adding hypothetical class of vibrational types of signatures – based on target and vibrational spectrum – this will correspond to the target hypothesis mean and covariance of $\mu_1(x)$ and $\Sigma_1(x)$ for the vector $\tilde{\mathcal{S}}_S(x)$

Step 4: Generate quadratic detection statistic based on Steps 2 and 3, which will be given as

$$\Lambda(x) = \left(\xi_S(x) - \mu_o(x) \right)^\top [\Sigma_o(x)]^{-1} \left(\xi_S(x) - \mu_o(x) \right) + \log(\det(\Sigma_o(x))) - \left(\xi_S(x) - \mu_1(x) \right)^\top [\Sigma_1(x)]^{-1} \left(\xi_S(x) - \mu_1(x) \right) - \log(\det(\Sigma_1(x)))$$

This is aligned with results in [4] and [5] which verifies that under appropriate conditions the cyclic spectral density has approximately Gaussian distribution with the appropriate mean and covariance formulas. In particular, it only need be approximately cyclostationary as specified in the latter reference. Also, it can be the case that the space of the cyclic frequencies which are in A_F , the interrogation set can be estimated relatively accurately based on latest results in references 3 and 4.

Dynamic Mode Decomposition

Koopman mode decomposition[6], [7], (KMD) is a recently-developed spectral decomposition method for the analysis of nonlinear systems, in which observable data is decomposed into modes with specific complex frequencies (corresponding to oscillation frequencies and/or growth and decay rates). KMD has been successfully applied to a wide range of dynamical systems, including fluid dynamics [8], neuroscience [9], and epidemiology [10], where the calculated Koopman modes' structure and time-dependent behavior can provide insight into the important characteristics of the nonlinear system.

The KMD of an observable g that is a function of time t and initial state space position z_0 is

$$g(t, z_0) = \sum_{j=1}^{\infty} e^{\lambda_j t} v_j(z_0) + e^{\bar{\lambda}_j t} \bar{v}_j(z_0)$$

where the λ_j are the complex Koopman eigenvalues, the v_j are the Koopman modes, and the overbar indicates complex conjugation. The complex eigenvalues consist of a real component, which determines the growth or decay of the given mode, and an imaginary component, which determines the oscillatory frequency of the mode.

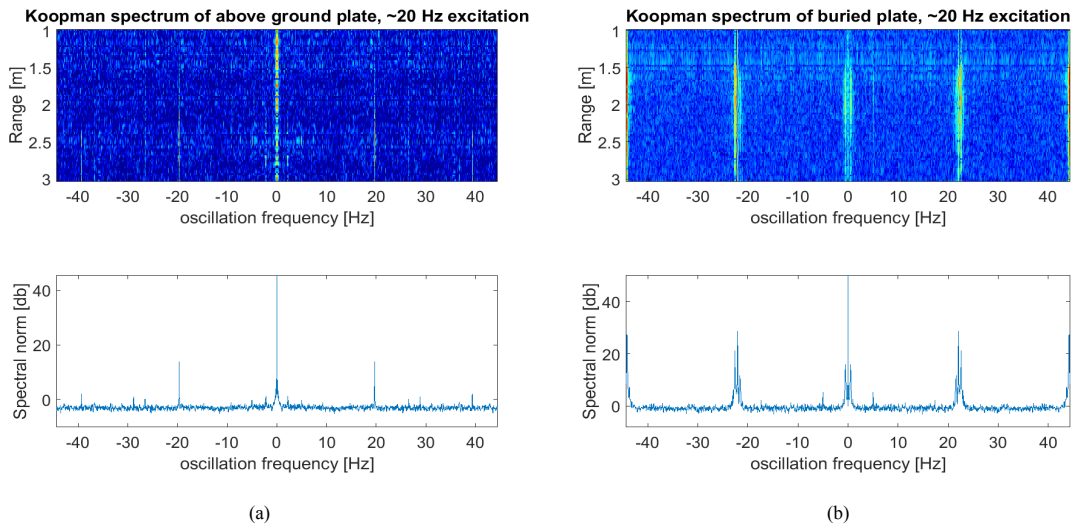


Figure 28. (a) shows the spectrum of above ground vibrating plate, (b) the below ground vibrating plate.

In the present system, KMD was considered an appropriate tool to detect the Doppler signal of the acoustically excited buried target. A particular advantage of KMD over Doppler analysis is the separation of Koopman modes both in frequency and in growth/decay. This offers the potential to distinguish between different signal sources at the same (or close by) frequencies, such as hardware noise and the return of an acoustically excited target that overlap in frequency. A pure Doppler spectrum would see only the sum of two such signals and thus mask their true nature, whereas the additional degree of freedom in the Koopman spectrum could allow separating the two signals by their growth/decay behavior (e.g. a transient hardware noise signal would have a large growth/decay rate, while the mode due to an acoustically excited buried target at a slowly change range would have a small growth/decay rate).

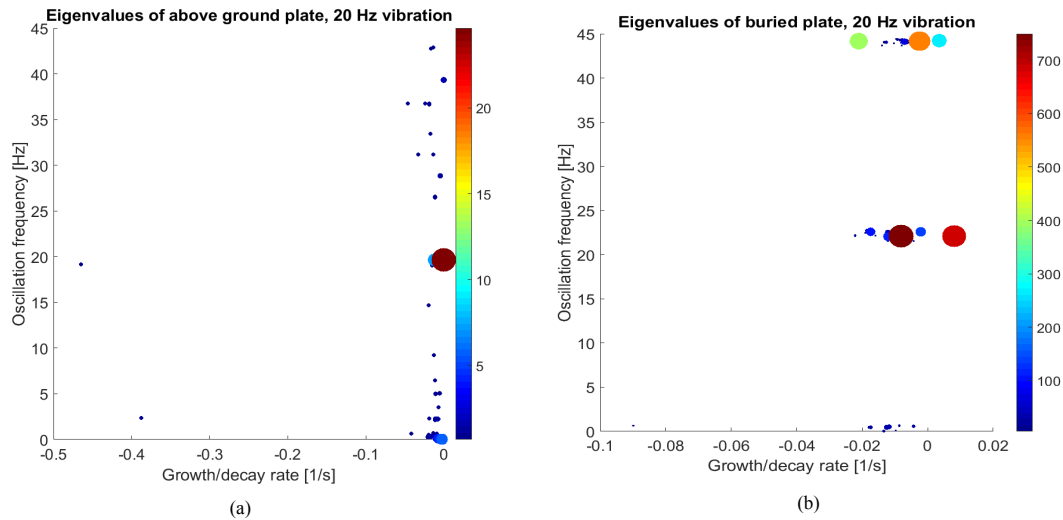


Figure 29 (a) shows the eigenvalues of the vibrating plate on the surface, (b) shows the eigenvalues of the buried plate.

Shown here are results of KMD of two measured datasets. The measured system consisted of a metal plate supported by springs in a frame. A mechanical excitation of approximately 20 Hz was applied to the plate to induce vibration. Fig. 11 shows, for both cases, the 2D Koopman spectra and 1D spectral norm (i.e. the norm along the range direction at each frequency). For the above ground case (Fig. 28(a)) the vibration of the plate at the excitation frequency is clearly visible at ± 20 Hz, as well as the harmonic at ± 40 Hz. In the buried case (Fig. 28(b)), the vibration due at the excitation frequency is still clearly visible, and the ± 40 Hz signal is significantly larger than the above ground case, believed to be due to the mixing products resulting from the reflection of the vibratory wave from the sand/air interface.

Fig. 29 shows the complex Koopman eigenvalues for the same two cases (for clarity, only the positive frequency part of the spectrum is shown. The negative frequency part is identical). These demonstrate the additional information content of the complex eigenvalues (consisting of growth/decay and oscillatory components) as compared to the purely oscillatory information obtained from Doppler/Fourier analysis. Each circle represents an eigenvalue, where the horizontal axis shows the real component of the eigenvalue and the vertical axis shows the imaginary component of the eigenvalue. The size and color of each circle shows the norm of the mode corresponding to that eigenvalue. In the above ground case (Fig. 29(a)), the largest norm modes (i.e. those with the most energy) are seen to be at the excitation frequency of 20 Hz and the 40 Hz harmonic, as well as near the 0 frequency DC value. The other eigenvalues are seen to primarily have negative growth rates and their associated modes have much smaller norms, therefore they can be identified as mostly due transient system effects or due to external sources.

The buried case (Fig. 28(b)) shows more complicated dynamics, as multiple eigenvalues corresponding to large norm modes are seen to exist at the 20 Hz excitation frequency and at the 40 Hz harmonic, and include both growing (positive horizontal axis value) and decaying (negative horizontal axis value) modes. This phenomenon is characteristic of buried vibrating objects and is caused by the damping effect of the soil medium on the plate vibration.

REFERENCES

- [1] C. T. Schröder, W. R. Scott, and G. D. Larson, “Elastic waves interacting with buried land mines: A study using the FDTD method,” *IEEE Trans. Geosci. Remote Sens.*, vol. 40, no. 6, pp. 1405–1415, 2002.
- [2] W. R. J. Scott, C. Schroeder, and J. S. Martin, “A hybrid acoustic/electromagnetic technique for locating land mines,” *IGARSS '98. Sens. Manag. Environ. 1998 IEEE Int. Geosci. Remote Sensing. Symp. Proceedings. (Cat. No.98CH36174)*, vol. 1, pp. 216–218, 1998.
- [3] V. C. Chen, F. Li, S.-S. Ho, and H. Wechsler, “Analysis of Micro-Doppler Signatures,” *IEE Proc. Radar, Sonar Navig.*, vol. 150, no. 4, pp. 271–276, 2003.
- [4] A. V Dandawate and G. B. Giannakis, “Statistical tests for presence of cyclostationarity,” *IEEE Trans. Signal Process.*, vol. 42, no. 9, pp. 2355–2369, 1994.
- [5] A. Napolitano, “Cyclic statistic estimators with uncertain cycle frequencies,” *IEEE Trans. Inf. Theory*, vol. XX, no. X, pp. 1–1, 2016.
- [6] I. Mezić and A. Banaszuk, “Comparison of systems with complex behavior,” *Phys. D Nonlinear Phenom.*, vol. 197, no. 1–2, pp. 101–133, 2004.
- [7] I. Mezić, “Spectral properties of dynamical systems, model reduction and decompositions,” *Nonlinear Dyn.*, vol. 41, no. 1–3, pp. 309–325, 2005.
- [8] I. Mezić, “Analysis of Fluid Flows via Spectral Properties of the Koopman Operator,” *Annu. Rev. Fluid Mech.*, vol. 45, no. 1, p. 121005161233001, 2012.
- [9] B. W. Brunton, L. A. Johnson, J. G. Ojemann, and J. N. Kutz, “Extracting spatial-temporal coherent patterns in large-scale neural recordings using dynamic mode decomposition,” *J. Neurosci. Methods*, vol. 258, pp. 1–15, 2016.
- [10] J. L. Proctor and P. A. Eckhoff, “Discovering dynamic patterns from infectious disease data using dynamic mode decomposition,” *Int. Health*, vol. 7, no. 2, pp. 139–145, 2015.

REPORT OF INVENTIONS AND SUBCONTRACTS
(Pursuant to "Patent Rights" Contract Clause) (See Instructions on back)

Form Approved
OMB No. 9000-0095
Expires Jan 31, 2009

The public reporting burden for this collection of information is estimated to average 1 hour per response, including the time for reviewing instructions, searching existing data sources, gathering and maintaining the data needed, and completing and reviewing the collection of information. Send comments regarding this burden estimate or any other aspect of this collection of information, including suggestions for reducing the burden, to the Department of Defense, Executive Services Directorate (9000-0095). Respondents should be aware that notwithstanding any other provision of law, no person shall be subject to any penalty for failing to comply with a collection of information if it does not display a currently valid OMB control number.

PLEASE DO NOT RETURN YOUR COMPLETED FORM TO THE ABOVE ORGANIZATION. RETURN COMPLETED FORM TO THE CONTRACTING OFFICER.

1. a. NAME OF CONTRACTOR/SUBCONTRACTOR AKELA Inc		c. CONTRACT NUMBER W911NF-16-P-0043		3. TYPE OF REPORT (X one) a. INTERIM <input type="checkbox"/> b. FINAL <input checked="" type="checkbox"/>	
b. ADDRESS (Include ZIP Code) 5551 Ekwill St Suite A Santa Barbara CA 93111		d. AWARD DATE (YYYYMMDD) 20160815		4. REPORTING PERIOD (YYYYMMDD) a. FROM 20160815 b. TO 20170214	
2. a. NAME OF GOVERNMENT PRIME CONTRACTOR Same as 1. a.		c. CONTRACT NUMBER Same as 1. c.			

SECTION I - SUBJECT INVENTIONS

5. "SUBJECT INVENTIONS" REQUIRED TO BE REPORTED BY CONTRACTOR/SUBCONTRACTOR (If "None," so state)		DISCLOSURE NUMBER, PATENT APPLICATION SERIAL NUMBER OR PATENT NUMBER		ELECTION TO FILE PATENT APPLICATIONS (X)		CONFIRMATORY INSTRUMENT OR ASSIGNMENT FORWARDED TO CONTRACTING OFFICER (X)	
a. NAME(S) OF INVENTOR(S) (Last, First, Middle Initial)	b. TITLE OF INVENTION(S)	c.	d.		e.		f.
			(1) UNITED STATES	(2) FOREIGN	(a) YES	(b) NO	
NONE							

f. EMPLOYER OF INVENTOR(S) NOT EMPLOYED BY CONTRACTOR/SUBCONTRACTOR		9. ELECTED FOREIGN COUNTRIES IN WHICH A PATENT APPLICATION WILL BE FILED	
(1) (a) NAME OF INVENTOR (Last, First, Middle Initial)	(2) (a) NAME OF INVENTOR (Last, First, Middle Initial)	(1) TITLE OF INVENTION	(2) FOREIGN COUNTRIES OF PATENT APPLICATION
(b) NAME OF EMPLOYER			
(c) ADDRESS OF EMPLOYER (Include ZIP Code)	(c) ADDRESS OF EMPLOYER (Include ZIP Code)		

SECTION II - SUBCONTRACTS (Containing a "Patent Rights" clause)

6. SUBCONTRACTS AWARDED BY CONTRACTOR/SUBCONTRACTOR (If "None," so state)		FAR "PATENT RIGHTS" d.		DESCRIPTION OF WORK TO BE PERFORMED UNDER SUBCONTRACT(S) e.		SUBCONTRACT DATES (YYYYMMDD) f.	
a. NAME OF SUBCONTRACTOR(S)	b. ADDRESS (Include ZIP Code)	c. SUBCONTRACT NUMBER(S)	d.		f.	g.	
			(1) CLAUSE NUMBER	(2) DATE (YYYYMM)		(1) AWARD	(2) ESTIMATED COMPLETION
Michigan Technological University	1400 Townsend Drive, Houghton MI, 49931-1295	AK-2016-0815	NA		Simulation and modeling development with algorithm development		

SECTION III - CERTIFICATION

7. CERTIFICATION OF REPORT BY CONTRACTOR/SUBCONTRACTOR (Not required if: (X as appropriate))		NONPROFIT ORGANIZATION	
I certify that the reporting party has procedures for prompt identification and timely disclosure of "Subject Inventions," that such procedures have been followed and that all "Subject Inventions" have been reported.		<input checked="" type="checkbox"/> SMALL BUSINESS or <input type="checkbox"/> NONPROFIT ORGANIZATION	
a. NAME OF AUTHORIZED CONTRACTOR/SUBCONTRACTOR OFFICIAL (Last, First, Middle Initial) Boutte, David, A	b. TITLE Senior Electrical Engineer	c. SIGNATURE David Boutte	d. DATE SIGNED 20170315